PCCP

PAPER

View Article Online
View Journal | View Issue

Cite this: *Phys. Chem. Chem. Phys.*, 2023, **25**, 20557

Distinguishing different surface interactions for nucleotides adsorbed onto hematite and goethite particle surfaces through ATR-FTIR spectroscopy and DFT calculations†

Izaac Sit,[a] Mark A. Young,[b] James D. Kubicki *[c] and Vicki H. Grassian *[b]

Geochemical interfaces can impact the fate and transport of aqueous species in the environment including biomolecules. In this study, we investigate the surface chemistry of adsorbed nucleotides on two different minerals, hematite and goethite, using infrared spectroscopy and density functional theory (DFT) calculations. Attenuated total reflectance-Fourier transform infrared spectroscopy is used to probe the adsorption of deoxyadenosine monophosphate (dAMP), deoxyguanosine monophosphate (dGMP), deoxycytidine monophosphate (dCMP), and deoxythymidine monophosphate (dTMP) onto either hematite or goethite particle surfaces. The results show preferential adsorption of the phosphate group to either surface. Remarkably, surface adsorption of the four nucleotides onto either hematite or goethite have nearly identical experimental spectra in the phosphate region (900 to 1200 cm^{-1}) for each mineral surface yet are distinctly different between the two minerals, suggesting differences in binding of these nucleotides to the two mineral surfaces. The experimental absorption frequencies in the phosphate region were compared to DFT calculations for nucleotides adsorbed through the phosphate group to binuclear clusters in either a monodentate or bidentate bridging coordination. Although the quality of the fits suggests that both binding modes may be present, the relative amounts differ on the two surfaces with preferential bonding suggested to be monodentate coordination on hematite and bidentate bridging on goethite. Possible reasons for these differences are discussed.

Received 16th March 2023,
Accepted 13th July 2023

DOI: 10.1039/d3cp01200j

rsc.li/pccp

Introduction

Goethite can represent 50–70% of the total surface area in soils.[1] Goethite is the most abundant iron oxyhydroxide and can be as much as 5 wt% in soils.[1] Hematite, is another common iron-containing soil component found in soil and in river waters.[1] In addition, both goethite and hematite are components of mineral dust aerosol.[2,3] Goethite and hematite particles can act as excellent adsorbents, simultaneously changing the physicochemical properties of the particle surfaces and affecting iron bioavailability.[4]

Previous studies have probed the interactions of oxyanions and other adsorbates on both iron oxide and iron oxyhydroxide surfaces.[5–16] Additionally, complexation at surfaces is also a function of pH. For example, Elzinga *et al.* probed phosphate adsorption onto hematite as a function of pH to measure different surface interactions.[10] Different binding modes occurred on the surface in the pH range between 3.5 to 8.9. From pH 3.5 to 7.0, a protonated monodentate structure was determined at high surface coverages and between pH 8.5 to 9.0, a deprotonated monodentate structure was present. For goethite, phosphate shows a bidentate complex between pH 4 and 6, and a monodentate complex between pH 7.5 to 7.9. Furthermore, in general, it is found that surface coverage is a function of pH. Lower pH favors more adsorption due to electrostatic interactions between the negatively charged oxyanion and positively charged surface.[7,10] These earlier studies show that iron mineral surface chemistry depends on solution phase pH, as well as surface composition and structure.

Insights into potentially different complexation modes can be facilitated by combining DFT calculations with experimental data. For example, Kubicki *et al.* investigated surface complexes of oxyanions with various iron and aluminum minerals by

[a] *Department of Nanoengineering, University of California San Diego, La Jolla, CA 92093, USA*
[b] *Department of Chemistry & Biochemistry, University of California San Diego, La Jolla, CA 92093, USA. E-mail: vhgrassian@ucsd.edu*
[c] *Department of Earth, Environmental & Resource Sciences, The University of Texas at El Paso, El Paso, TX 79968, USA. E-mail: jdkubicki@utep.edu*

† Electronic supplementary information (ESI) available: Supplementary Information is available and contains one figure and three tables. Goethite particle characterization data (Fig. S1). The tables include: zeta potential measurements (Table S1) and calculated *versus* experimental frequencies in the 900 to 1200 cm^{-1} spectral region for dAMP and dGMP (Table S2) and for dCMP and dTMP (Table S3). See DOI: https://doi.org/10.1039/d3cp01200j

comparing experimental frequencies with DFT-calculated frequencies for binuclear metal clusters.[11] Notably, phosphate complexation with goethite demonstrated a pH dependence whereby a bidentate species was prevalent under acidic conditions and a monodentate binding motif was present under more basic conditions. However, when these results were compared to similar studies by Arai and Sparks[12] and Persson *et al.*[13] there were distinct differences, suggesting that surface adsorption can depend on particle size and the presence of different surface planes.[15–17] In particular, differences in particle synthesis, composition and morphology can result in lattice and edge defects that then lead to preferential adsorption on specific planes.[17] Additionally, in another study by Kubicki *et al.*, it was determined that there were different adsorption energies for different surface complexation modes for phosphate adsorbed onto goethite on different lattice planes using Gaussian 16 calculations.[5] The results suggested that an inner-sphere bidentate coordination was favored and preferential on the (101) and (100) plane but unfavorable on (001) whereas monodentate coordination was preferential on the (210) and (001) planes.

These studies for relatively simple inorganic oxyanions show that the chemistry on surfaces is complex and that the complexation modes depend on multiple factors. Thus, studies of more complex molecules is even more challenging.[18–21] For example, in terms of environmental relevance, nucleotides, and environmental DNA (or eDNA) can be readily found in aqueous systems through active cellular secretion or apoptosis.[22] The availability of biomolecules and essential nutrients in solution is heavily impacted by adsorption.[23,24] Additionally, large biomacromolecular structures, like DNA, have been suggested to be stabilized on surfaces with increased persistence in aqueous environments through different biomes, providing a source of genetic information for gene transfer.[22] The conformation of DNA is related to the preferential adsorption of the phosphate backbone to various mineral surfaces. Schmidt and Martinez adsorbed DNA onto goethite and were able to show that there was no change to DNA form which retained the B-form conformation that is measured in solution.[25] Recently, Sit *et al.* showed interesting results for DNA adsorbed onto hematite. In particular, although the ATR-FTIR spectrum of DNA in the solution phase was consistent with the B-form, it appeared that upon adsorption there was a conformational change to the Z-form.[26] These results suggest that there may be differences between goethite and hematite that warrant further study on exactly how the phosphate backbone of DNA interacts with different iron-containing minerals. However, it may be desirable to first better understand how monomeric units of DNA, *i.e.* nucleotides, interact with these mineral surfaces. From such studies, knowledge of how these important building blocks interact with particle surfaces can lay the foundation for larger macromolecules. Previous studies have shown that deoxyadenosine monophosphate and adenosine monophosphate preferentially bind to metal oxide surfaces, such as anatase, rutile, and alumina, *via* the phosphate group rather than the ribose and nitrogenous rings.[7,27–30] However, these surfaces, although found in the environment, are not as common as iron oxides and oxyhydroxides and studies such as the ones done here can provide some of the fundamental science needed to understand the lifetime and fate of adsorbed eDNA.

In this study, we probe the adsorption of four nucleotides, deoxyadenosine monophosphate (dAMP), deoxyguanosine monophosphate (dGMP), deoxycytidine monophosphate (dCMP), and deoxythymidine monophosphate (dTMP), on both hematite and goethite particle surfaces at pH 5, a pH value below the pzc for these minerals.[31] This pH was chosen as it is the pH where the greatest amount of adsorption occurs. Attenuated total reflectance-Fourier transform infrared (ATR-FTIR) spectroscopy is used as an experimental probe to follow the adsorption process in real time. We compare the phosphate experimental frequencies to *ab-initio* frequencies for monodentate or bidentate biding modes on a binuclear iron cluster. The experimental data clearly show that all four nucleotides have similar coordination modes on each of the particle surface types interrogated but that there are differences in the coordination modes, most likely differences in the amounts of monodentate *versus* bindentate for hematite compared to goethite.

Materials and methods

Materials

2′-deoxyadenosine-5′-monophopshate (dAMP), 2′-deoxyguanosine-5′-monophosphate (dGMP), 2′-deoxycytidine-5′-monophosphate (dCMP), 2′-deoxythmidine-5′-monophosphate (dTMP), sodium chloride, 1N hydrochloric acid, and 1N sodium hydroxide were purchase from Sigma-Aldrich (where 1N means 1 normal concentrations of these solutions). Hematite and goethite particles were purchased from Alfa Aesar, MA. Zeta potential measurements of nucleotides at pH 5 were performed with the Zetasizer Nano from Malvern Instruments. Triplicate measurements are reported with 1σ standard deviation for the indicated error.

Particle characterization

The crystalline phase of iron oxide particles was determined with X-ray diffraction using an APEX II ultra-diffractometer with Mo Kα radiation at λ = 0.70930 Å. To determine the primary iron oxide particle sizes, an aqueous suspension of a 0.01 g L^{-1} was sonicated with a probe sonicator for 60 seconds in a room temperature water bath. Afterwards, a 15 uL aliquot was drop-casted onto a formvar/carbon-coated 100 mesh copper grid and dried. The copper grid was imaged using an 80 kV JEOL-1400 Plus transmission electron microscope. Particle sizes were analyzed using ImageJ software for more than 70 particles. Specific surface area was determined using a Quantachrome Nova 4200e N_2 adsorption isotherm under liquid nitrogen. Samples were first degassed at 80 °C for 18 hrs and a 15-multipoint isotherm was collected between P/P_0 of 0.05–0.95.

Attenuated total reflectance Fourier transform infrared (ATR-FTIR) spectroscopy

The ATR-FTIR spectroscopy setup has been previously described.[7,20,26,32] Briefly, ATR-FTIR spectroscopy is based on the total internal reflection of an infrared beam at the interface

between a high index medium (ATR crystal) and low index medium (aqueous sample). The reflection of the infrared beam at the interface creates an exponentially decaying evanescent wave that propagates into the sample where absorption of light occurs. The ATR accessory was a horizontal flow cell equipped with an amorphous material transmitting IR radiation (AMTIR) crystal. The infrared spectrophotometer is a Nicolet iS10 FTIR (Thermo-Fisher) equipped with a mercury cadmium telluride detector (MCT/A). Spectra were collected at a resolution of 4 cm^{-1} averaged over 100 scans in the spectra range of 750 to 4000 cm^{-1}. All ATR-FTIR spectra were collected with OMNIC 9 software and linearly baseline corrected between 900 to 1800 cm^{-1}.

For single component solution phase spectra, separate solutions of 2 mM dAMP, 2 mM dGMP, 2 mM dCMP, and 2 mM dTMP were prepared in 10 mM NaCl and titrated to pH 5 using NaOH or HCl. A solution of 2 mM dAMP was pipetted onto the ATMIR crystal and a spectrum was collected using a background of 10 mM NaCl. Similar solution phase spectra were collected for the other three nucleotides.

For single component adsorption on hematite particles, a particle film was prepared by sonicating 2.5 mg α-Fe_2O_3 in 700 uL of Milli-Q water and drop casting the colloidal suspension onto the AMTIR crystal. The suspension was left to dry overnight resulting in a uniform particle film. A solution of 10 mM NaCl at pH 5 was flowed over the film using a peristaltic pump at $\sim$1 mL min^{-1} to remove loose particles and collect a background spectrum. A 20 uM nucleotide solution in 10 mM NaCl titrated to pH 5 was flowed over the film for 180 minutes. Although this is higher than typical values found for eDNA in the environment,[33] these studies are meant to probe how these molecules adhere to iron oxide particle surfaces. To facilitate desorption, a flow of a solution of 10 mM NaCl over the film at pH 5 began while spectra were collected at increments of 2.5 minutes. This was done for all four nucleotides. The same method was performed for single component adsorption on goethite particle surfaces using 2.5 mg α-FeOOH. A desorption spectrum was collected after flowing pure pH 5 water over the crystal film for two hours.

DFT calculations

Model complexes of dAMP were bonded to an Fe-hydroxide cluster as a bidentate complex, $[Fe_2(OH)_4(OH_2)_4dAMP{\cdot}(H_2O)_6]$, and a monodentate complex, $[Fe_2(OH)_5(OH_2)_4dAMP{\cdot}(H_2O)_6]$. The clusters have six explicit H_2O molecules to represent hydrogen bonding interactions. Modeled clusters were energy minimized without symmetry or geometrical constraints with B3LYP functionals[34,35] and the 6-31G(d) basis set using Gaussian 16.[36] Vibrational frequencies were scaled by a factor of 0.960.[37] Although it is possible to model explicit surfaces of minerals and the associated surface complexes,[5,38] the data in this case do not justify extensive calculations on a variety of surfaces because the IR spectra are consistent within each mineral. Comparisons of model IR frequencies derived from periodic simulations and cluster calculations such as those employed here indicate that clusters provide similar results to the more expensive and time-consuming periodic simulations.[37,39] Furthermore, the cluster calculations derive analytical frequencies and IR/Raman intensities compared to the numerical frequencies obtained in periodic calculations.

Results and discussion

Particle characterization

Hematite particles have been previously characterized.[20] Briefly, α-Fe_2O_3 was confirmed to be hematite with XRD with particle size

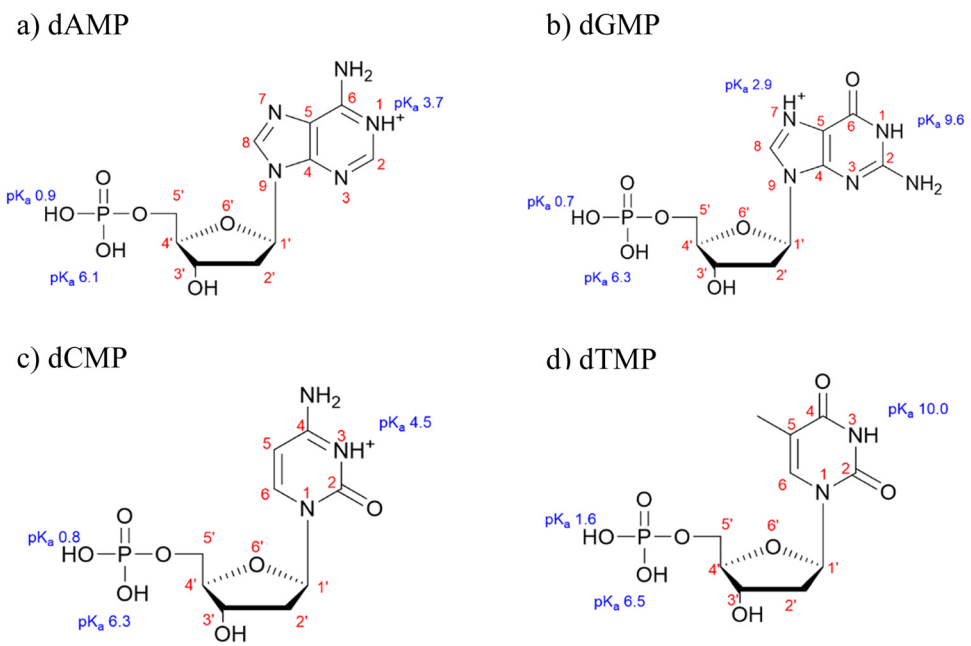

Fig. 1 Molecular structures for (a) deoxyadenosine monophosphate (dAMP), (b) deoxyguanosine monophosphate (dGMP), (c) deoxycytidine monophosphate (dCMP), and (d) deoxythymidine monophosphate (dTMP) with pK_a values from ref. 40.

Table 1 Percent speciation table for deoxyadenosine monophosphate (dAMP), deoxyguanosine monophosphate (dGMP), deoxycytidine monophosphate (dCMP), and deoxythymidine monophosphate (dTMP) at in solution at pH 5 using the Henderson–Hasselbalch equation $\left(\mathrm{pH} = \mathrm{p}K_a + \log\left(\frac{[\mathrm{A}^-]}{[\mathrm{HA}]}\right)\right)$

	dX^+MP^-	$dXMP^-$	$dXMP^{2-}$
dAMP	4.4	88.6	7.0
dGMP	0.8	94.5	4.7
dCMP	23.1	73.2	3.7
dTMP	0.0	96.9	3.1

of 5 to 20 nm in diameter and specific surface area of 75.7 ± 8.2 $m^2\ g^{-1}$. Goethite particle phase was confirmed with XRD, with an average rod-like particle size of 388 ± 167 nm by 87 ± 29 nm (Fig. S1 in ESI†). The specific surface area was measured to be 38 ± 12 $m^2\ g^{-1}$.

Analysis of solution and adsorbed spectra

Fig. 1 shows the molecular structures of the fully protonated forms of dAMP, dGMP, dCMP, and dTMP along with the pK_a values of the phosphate group and nitrogenous rings.[40] dAMP and dGMP are comprised of a purine ring while dCMP and dTMP contain a pyrimidine ring. The speciation of all four nucleotides at pH 5 is listed in Table 1. At pH 5, the major form of all four nucleotides is a monovalent anionic form with minor contributions from a zwitterionic and divalent anionic species. These negatively charged nucleotides are reflected in the zeta potential measurements that range from −6 to −9 mV for all four nucleotides (Table S1 in ESI†). Solution phase spectral features are discussed in detail elsewhere.[30] Briefly, absorption in the region between 1200 to 1800 cm^{-1} can be assigned to the nucleoside group whereas features in the 900 to 1200 cm^{-1} range can be attributed to the phosphate group. Between all four nucleotides, the 1200 to 1800 cm^{-1} region is spectrally unique, whereas the 900 to 1200 cm^{-1} region can be similar because this is the region where the phosphate group absorptions are and the pK_as are close.

The solution phase spectra can be compared to adsorbed spectra and any spectral differences can be attributed to nucleotide interactions with the particle surface. Fig. 2 shows the temporal evolution of the spectra for adsorbed purine nucleotides on both hematite and goethite particles. Overall, we observe a significant increase in intensity when the nucleotides are adsorbed onto either surface when compared to solution. The adsorbed spectral intensities are thirty times larger than in the solution, despite the 100 times higher solution phase concentration. Consequently, the spectra are dominated by adsorbed nucleotides with minimal contributions from solution phase species. When comparing the dAMP nucleoside 1200 to 1800 cm^{-1} region in solution to adsorbed spectra on either hematite or goethite, there is minimal peak

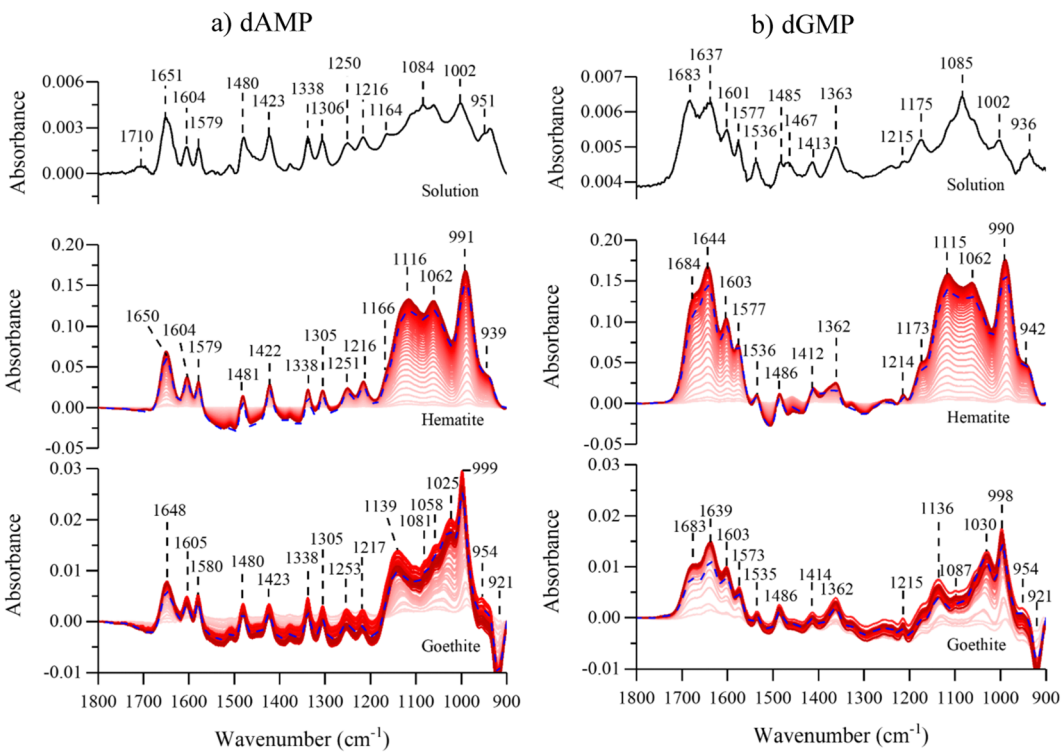

Fig. 2 ATR-FTIR purine spectra for (a) dAMP and (b) dGMP in solution (top), adsorbed on hematite (middle), and adsorbed on goethite (bottom). For these adsorbate spectra, lighter red color spectra represent earlier time points where darker lines represent later time points until 180 min. Although spectra were collected every 2.5 minutes only every other spectra have been plotted. The blue dotted line represents the desorption spectra for each nucleotide and shows that there is mostly irreversible adsorption at pH 5. The desorption spectra were obtained after flowing pure aqueous solution at pH 5 for 120 minutes. Background spectra were for the mineral surface in aqueous phase at pH 5.

shifting or broadening. However, there is a surface induced deprotonation of the nucleoside, as noted by the disappearance of the 1710 cm^{-1} $N1H^{+}$ feature upon adsorption to both hematite and goethite particles. This has been previously observed on anatase and hematite particles.[7,30] For dGMP, minimal spectral differences are observed in the nucleoside region, upon adsorption onto either hematite or goethite. A vibrational mode assignment for the spectral region from 1200 to 1800 cm^{-1} is provide in Table S2 (ESI†) for solution phase and adsorbed dAMP and dGMP.[7,30,41–46] When the nucleotides are adsorbed onto hematite or goethite, the 900 to 1200 cm^{-1} phosphate region broadens and undergoes peak shifting. Previous studies have observed the preferential adsorption of the phosphate group over the nitrogenous nucleobases to various surfaces for nucleotides, oligonucleotides, and DNA.[5,30–35] This suggests that the nucleotides are directly bound to these iron surfaces *via* the phosphate group.

Fig. 3 shows the pyrimidine ATR-FTIR nucleotide spectra in solution and adsorbed onto hematite or goethite. When the nucleoside regions are compared between solution and adsorbed on either particle surface for both nucleotides, there are minimal differences. Interestingly, dCMP does not undergo a nucleoside deprotonation, as was observed for dAMP. Surface induced deprotonation for dAMP but not for dCMP has been previously observed on anatase particles.[30] A vibrational mode assignment for dCMP and dTMP in the spectral region from 1200 to 1800 cm^{-1} is provide in Table S3 (ESI†).[7,30,41–46] Similar to what was observed for the purine nucleotides, the adsorbed phosphate absorption bands between 900 to 1200 cm^{-1} are broadened and shifted compared to the solution spectra and discussed in more detail below. Similar conclusions can be made about the pyrimidine nucleotides being directly bound to the iron surfaces *via* the phosphate group.

Comparison spectra of the four different adsorbed nucleotides on hematite and goethite are shown in Fig. 4a and b, respectively. These spectra were recorded after 180 minutes of adsorption, the last time point in red shown in Fig. 2 and 3. On hematite, the phosphate spectral region between 900 to 1200 cm^{-1} is similar for all four nucleotides and on goethite, the phosphate spectral region is also similar for all four nucleotides. Of particular significance is that when the phosphate region is compared between hematite and goethite particles, the regions are found to be spectrally distinct. Sit *et al.* showed that adsorbed nucleotides on TiO_2 and the phosphate regions manifested similar spectral shapes regardless of the nucleobase derivative.[30] Because the phosphate spectral band shapes are different between the two particles, this would suggest there are differences in adsorption to the surface and additional analysis is needed to identify relevant binding modes.

Comparison of calculated to experimental phosphate vibrational frequencies

Ab-initio calculations were carried out to better understand the adsorption of nucleotides and rationalize the observed

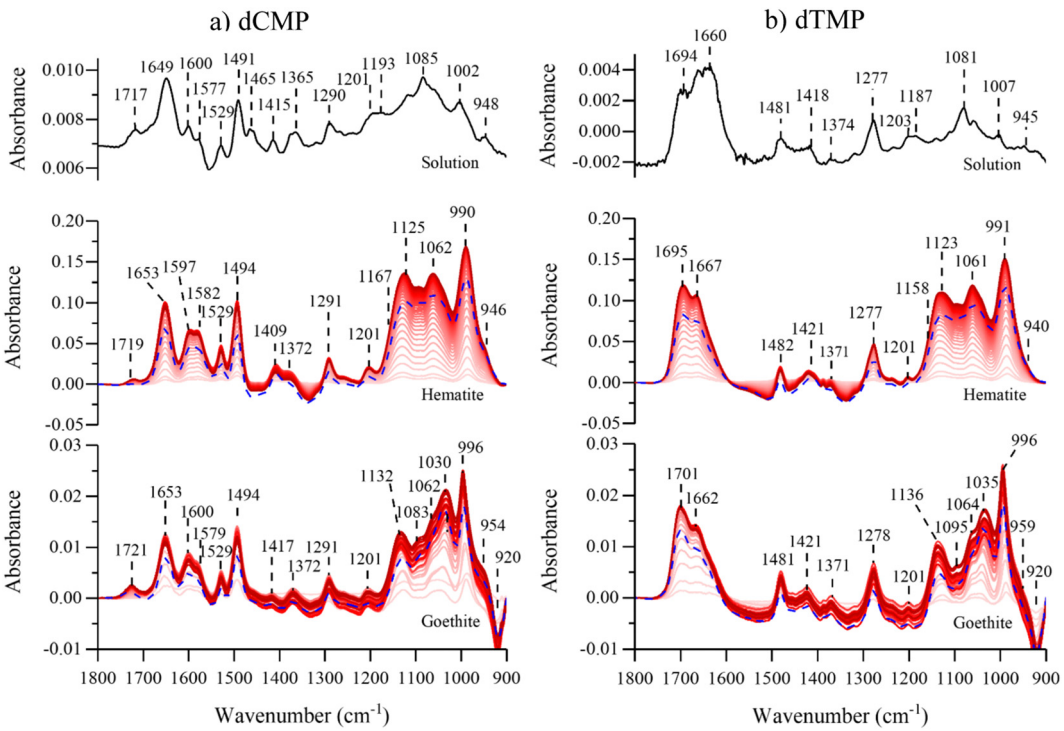

Fig. 3 ATR-FTIR pyrimidine spectra for (a) dCMP and (b) dTMP in solution (top), adsorbed on hematite (middle), and adsorbed on goethite (bottom). For these adsorbate spectra, lighter red color spectra represent earlier time points where darker lines represent later time points until 180 min. Although spectra were collected every 2.5 minutes only every other spectra have been plotted. The blue dotted line represents the desorption spectra for each nucleotide and shows that there is a mostly irreversible adsorption. The desorption spectra were obtained after flowing pure aqueous solution at pH 5 for 120 minutes. Background spectra were for the mineral surface in aqueous phase at pH 5.

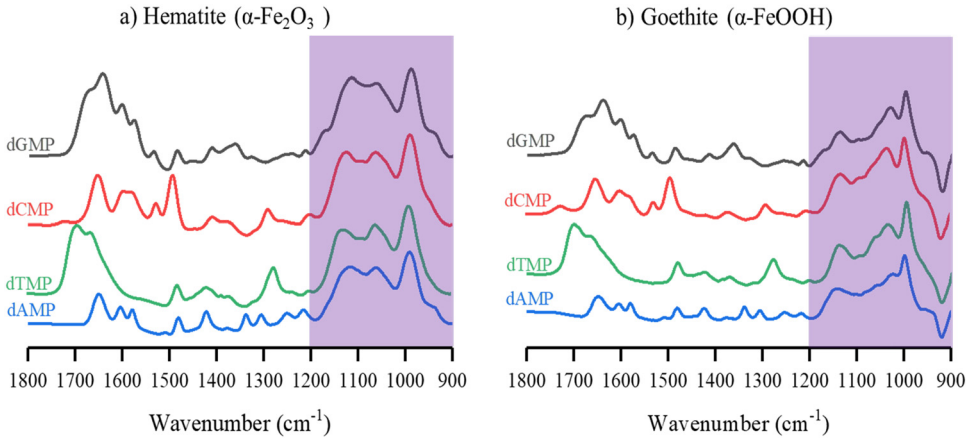

Fig. 4 ATR-FTIR normalized spectra of dAMP, dGMP, dCMP and dTMP adsorbed onto (a) hematite and (b) goethite after 180 minutes of adsorption. The phosphate region is shaded to highlight the similarities found for the phosphate spectral reaction for each of the adsorbed nucleotides on a particular mineral surface.

differences between hematite and goethite spectra. Since all nucleotide spectra look similar on each of the surfaces, we have investigated only one of the nucleotides, dAMP, bound to a binuclear iron cluster in two different coordination states: an inner-sphere monodentate complex and a bidentate bridging complex as shown in Fig. 5. dAMP was used as the model nucleotide as it can be compared to previous literature reports. The use of small metal clusters to model binding modes has been previously done with success and a similar approach is employed here.[10] A previous study found that increasing coordinating waters from 6 to 18 did not significant change the resulting spectrum, so six water molecules were used in the calculation here.[26] Additionally, because the goal is to model the phosphate binding mode, the coordinating water hydrated the phosphate and iron oxide cluster.

The calculated monodentate and bidentate dAMP phosphate region frequencies can be compared to both experimental hematite and goethite frequencies. First the experimental data were curve fit in the 900 to 1200 cm^{-1} spectral region for both hematite and goethite. These data are shown in Fig. 6 for dAMP on hematite and goethite.

A comparison between calculated (scaled) and experimental peak positions can be found in Fig. 7 and Table 2. (Note: due to curve fitting, some of the frequencies listed in Table 2 differ slightly from that shown in Fig. 2 in the 900 to 1200 cm^{-1} spectral region.) Three criteria were used to determine the best fit for each dominant surface complexation mode: (i) a slope closest to one; (ii) a y-intercept closest to zero; and (iii) $R >$ 90%. For hematite (Fig. 7a), the monodentate structure gives the better fit for these criteria. For goethite (Fig. 7b), the fitting

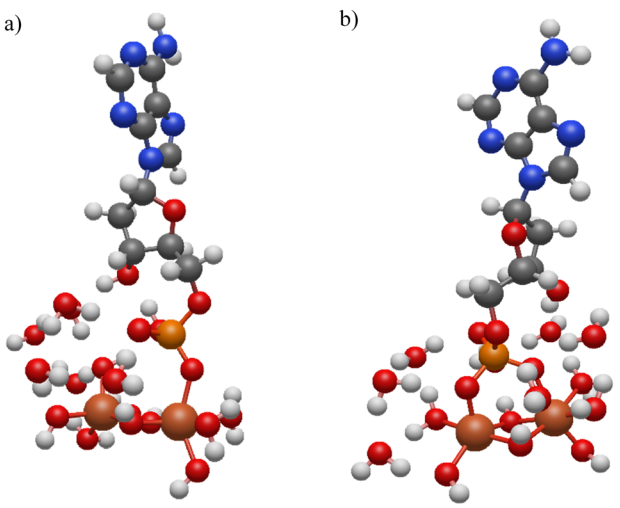

Fig. 5 DFT calculated structures for dAMP adsorbed onto iron cluster in (a) monodentate and (b) bidentate binding modes. Atom colors are the following: carbon (gray), hydrogen (white), nitrogen (blue), oxygen (red), phosphorous (orange), and iron (dark orange).

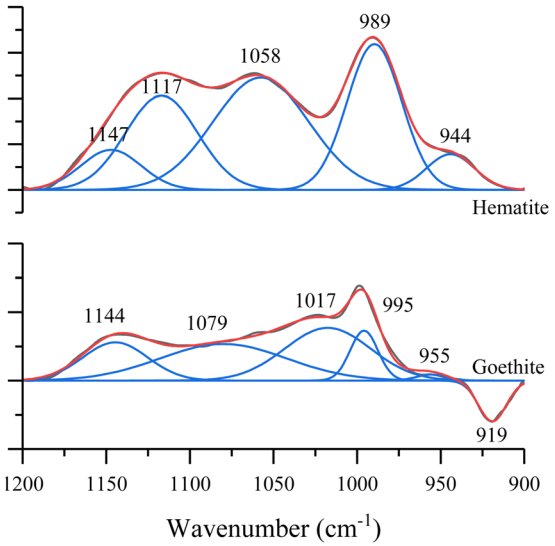

Fig. 6 Spectral curve fitting in the 900 to 1200 cm^{-1} region for dAMP adsorbed on hematite and goethite. The negative peak in the goethite spectrum comes from the goethite absorption band.

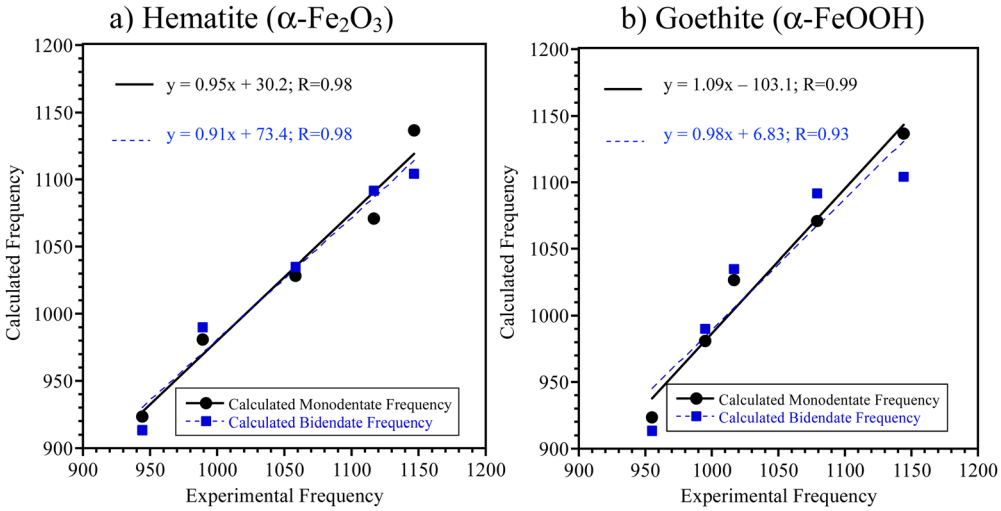

Fig. 7 Correlation between ATR-FTIR experimental and Gaussian calculated frequencies for monodentate (black circles) and bidentate (blue squares) coordination modes in the phosphate spectral region from 900 to 1200 cm^{-1} for dAMP adsorbed onto (a) hematite and (b) goethite. Linear fits to the data are shown.

parameters for the slope and *y*-intercept suggest that bidentate is the dominant binding mode. Although, these DFT calculations point towards this current interpretation to explain the spectral differences, they do not definitively resolve the assignments. Instead, these relatively closely fitted parameters suggest the presence of multiple binding modes but with different relative contributions to the overall spectra.

The computational results along with the experimental data presented here suggest that the different particle surfaces give rise to different coordination modes for the relevant nucleotides or, at the very least, different amounts of each of these different coordination modes. Similarly, Feuillie *et al.* also showed multiple coordinate modes for ribonucleotides adsorbed on corundum (α-Al_2O_3) surfaces with mostly monodendate complexation at pH 5 with a smaller amount of bidendate complexation.[28] For hematite, which has similar structure to corundum, this is what is proposed here as well. Our experimental results are clear in that the surface adsorption is similar for all four nucleotides adsorbed on either hematite or goethite but differ between the two mineral surfaces as shown in the experimental data by the different intensities of the different absorption bands in the 900 to 1200 cm^{-1} spectral region. These results taken together show that surface interactions and complexation with nucleotides differ for these two phases of iron-mineral particles based on the differences in the infrared spectra.

Overall, these results agree with many other studies in the literature that have shown differences in the properties and adsorption behavior between hematite particle surfaces compared to goethite particle surfaces. In particular, experimental and theoretical investigations have pointed toward several differences including surface structures, surface hydroxyl group densities, and surface coordination for these two minerals.[47–49] Other differences between hematite and goethite include heterogeneities of surface structure due to different sample preparations and size-dependent energetics.[50] Most relevant to this study, is that these differences result in hematite and goethite having different interactions with adsorbates including its interactions with water[50] as well as inorganic and organic phosphates.[51,52] Furthermore, due to the heterogeneity found for hematite particles relative to goethite, these results can be very sample dependent. Overall, our study points to different interactions of nucleotides with the two different mineral investigated here.

Because of this complexity, it can be difficult to pinpoint the exact reasons behind the origin of the different interactions of these two minerals with adsorbates. These differences are potentially due to the spatial arrangement and interatomic

Table 2 Calculated *versus* curve-fit, experimental frequencies in the 900 to 1200 cm^{-1} spectral region for dAMP adsorbed onto hematite *versus* goethite

Experimental frequencies (cm^{-1})		Calculated frequencies (cm^{-1}) and mode assignments			
Hematite	Goethite	Monodendate	Monodendate mode assignment	Bidentate	Bidendate mode assignment
944	955	923	δ(P–OH)	913	$\nu(PO_4)$
989	995	981	δ(P–OH) and ν(PO–C)	990	$\nu(PO_4)$ and ν(PO–C)
1058	1017	1027	$\nu(PO_4)$ + sugar ring	1035	$\nu(PO_4)$ and ν(PO–C)
1117	1079	1071	$\nu(PO_4)$ + sugar ring	1092	$\nu(PO_4)$ + sugar ring
1147	1144	1137	$\nu(PO_4)$	1104	$\nu(PO_4)$ + sugar ring

distances between Fe atoms of the different surface planes for hematite and goethite. Specifically, Villalobos and Perez-Gallegos[53] observed that for chromate (which behaves similar to phosphate) adsorption to goethite "a predominance of (210) and/or (010) faces explains the high reactivity of low surface area goethite." The (210) and (010) surfaces which have higher densities of singly-terminated Fe–O sites compared to the (101) and (001) surfaces. The singly-terminated Fe–O sites are close enough to each other on the (010) surface that bidentate bonding is possible in this case although for phosphate[38] and phosphodiesters likely form monodentate complexes.[54] The number of contiguous singly-coordinated Fe–O groups can control whether or not bidentate bridging complexes form, and Barron and Torrent[47] have shown that the goethite has surfaces with a higher site densities of these groups.

Most importantly, studies of nucleotide adsorption can potentially provide insights into the conformation and binding of eDNA on relevant mineral surfaces. Additional experimental and computational efforts will be needed to fully address the connection between nucleotides adsorption and eDNA adsorption. The current work represents a first step towards understanding how different Fe-containing minerals can interact with these smaller biological subunits.

Conclusions

Herein, we have combined experimental spectroscopic data and *ab-initio* calculations to show that the interaction of selected nucleotides on two iron-mineral surfaces, goethite and hematite, is different. The data indicate there are two modes of binding, monodentate and bidendate, and that monodendate binding mode may be preferred on hematite while bidentate mode may be favored on goethite, although both modes are most likely present on the two different mineral surfaces but of different relative amounts. Overall, this study provides a framework towards a more complete understanding regarding the behavior of more complex macromolecules, like eDNA, by investigating the surface adsorption of monomeric, nucleotide subunits.

Conflicts of interest

There are no conflicts to declare.

Acknowledgements

We thank Eleanor Quirk and Dr Eshani Hettiarachchi with data collection. The research reported here was funded in whole or in part by the Army Research Office/Army Research Laboratory (W911NF-19-1-0078 and W911NF-23-1-0181) to the University of California, San Diego. Any errors and opinions are not those of the Army Research Office or Department of Defense and are attributable solely to the author(s). The TEM images were acquired at University of California, San Diego - Cellular and Molecular Medicine Electron Microscopy Core (UCSD-CMM-EM Core) for equipment access and technical assistance. The UCSD-CMM-EM Core is supported in part by the National Institutes of Health Award number S10OD023527. This research was supported in part by W. M. Keck Foundation through computing resources at the W. M. Keck Laboratory for Integrated Biology at UCSD. M. Keck Laboratory for Integrated Biology at UCSD.

References

1 U. Schwertmann, R. M. Taylor, J. B. Dixon and S. B. Weed, *Minerals in Soil Environments*, ed. J. B. Dixon, S. B. Weed, Soil Science Society of America, Madison, Wisconsin, EUA, 1989, p. 379.
2 E. Journet, Y. Balkanski and S. P. Harrison, A New Data Set of Soil Mineralogy for Dust-Cycle Modeling, *Atmos. Chem. Phys.*, 2014, **14**, 3801–3816.
3 S. Go, A. Lyapustin, G. L. Schuster, M. Choi, P. Ginoux, M. Chin, O. Kalashnikova, O. Dubovik, J. Kim, A. da Silva, B. Holben and J. S. Reid, Inferring iron-oxide species content in atmospheric mineral dust from DSCOVR EPIC observations, *Atmos. Chem. Phys.*, 2022, **22**, 1395–1423.
4 J. Baltrusaitis, D. M. Cwiertny and V. H. Grassian, Adsorption of Sulfur Dioxide on Hematite and Goethite Particle Surfaces, *Phys. Chem. Chem. Phys.*, 2007, **9**, 5542–5554.
5 J. D. Kubicki, K. W. Paul, L. Kabalan, Q. Zhu, M. K. Mrozik, M. Aryanpour, A.-M. Pierre-Louis and D. R. Strongin, ATR–FTIR and Density Functional Theory Study of the Structures, Energetics, and Vibrational Spectra of Phosphate Adsorbed onto Goethite, *Langmuir*, 2012, **28**, 14573–14587.
6 X. Huang, X. Hou, X. Zhang, K. M. Rosso and L. Zhang, Facet-Dependent Contaminant Removal Properties of Hematite Nanocrystals and Their Environmental Implications, *Environ. Sci.: Nano*, 2018, **5**, 1790–1806.
7 I. Sit, S. Sagisaka and V. H. Grassian, Nucleotide Adsorption on Iron(III) Oxide Nanoparticle Surfaces: Insights into Nano–Geo–Bio Interactions Through Vibrational Spectroscopy, *Langmuir*, 2020, **36**, 15501–15513.
8 K. D. Kwon and J. D. Kubicki, Molecular Orbital Theory Study on Surface Complex Structures of Phosphates to Iron Hydroxides: Calculation of Vibrational Frequencies and Adsorption Energies, *Langmuir*, 2004, **20**, 9249–9254.
9 E. Kumar, A. Bhatnagar, W. Hogland, M. Marques and M. Sillanpää, Interaction of Inorganic Anions with Iron-Mineral Adsorbents in Aqueous Media—A Review, *Adv. Colloid Interface Sci.*, 2014, **203**, 11–21.
10 E. J. Elzinga and D. L. Sparks, Phosphate Adsorption onto Hematite: An in Situ ATR-FTIR Investigation of the Effects of pH and Loading Level on the Mode of Phosphate Surface Complexation, *J. Colloid Interface Sci.*, 2007, **308**, 53–70.
11 J. D. Kubicki, K. D. Kwon, K. W. Paul and D. L. Sparks, Surface Complex Structures Modelled with Quantum Chemical Calculations: Carbonate, Phosphate, Sulphate, Arsenate and Arsenite, *Eur. J. Soil Sci.*, 2007, **58**, 932–944.

12 Y. Arai and D. L. Sparks, ATR–FTIR Spectroscopic Investigation on Phosphate Adsorption Mechanisms at the Ferrihydrite–Water Interface, *J. Colloid Interface Sci.*, 2001, **241**, 317–326.
13 P. Persson, N. Nilsson and S. Sjöberg, Structure and Bonding of Orthophosphate Ions at the Iron Oxide–Aqueous Interface, *J. Colloid Interface Sci.*, 1996, **177**, 263–275.
14 S. Soldoozy, A. Trinh, J. D. Kubicki and H. A. Al-Abadleh, In situ and Real-Time ATR-FTIR Temperature-Dependent Adsorption Kinetics Coupled with DFT Calculations of Dimethylarsinate and Arsenate on Hematite, *Langmuir*, 2020, **36**, 4229–4307.
15 M. Villalobos, I. N. Escobar-Quiroz and C. Salazar-Camacho, The Influence of Particle Size and Structure on the Sorption and Oxidation Behavior of Birnessite: I. Adsorption of As(V) and Oxidation of As(III), *Geochim. Cosmochim. Acta*, 2014, **125**, 564–581.
16 C. Salazar-Camacho and M. Villalobos, Goethite Surface Reactivity: III. Unifying Arsenate Adsorption Behavior through a Variable Crystal Face – Site Density Model, *Geochim. Cosmochim. Acta*, 2010, **74**, 2257–2280.
17 K. J. T. Livi, M. Villalobos, R. Leary, M. Varela, J. Barnard, M. Villacís-García, R. Zanella, A. Goodridge and P. Midgley, Crystal Face Distributions and Surface Site Densities of Two Synthetic Goethites: Implications for Adsorption Capacities as a Function of Particle Size, *Langmuir*, 2017, **33**, 8924–8932.
18 M. P. Schmidt and C. E. Martínez, Supramolecular Association Impacts Biomolecule Adsorption onto Goethite, *Environ. Sci. Technol.*, 2018, **52**, 4079–4089.
19 M. P. Schmidt and C. E. Martinez, Kinetic and Conformational Insights of Protein Adsorption onto Montmorillonite Revealed Using in Situ ATR-FTIR/2D-COS, *Langmuir*, 2016, **32**, 7719–7729.
20 I. Sit, Z. Xu and V. H. Grassian, Plasma Protein Adsorption on TiO_2 Nanoparticles: Impact of Surface Adsorption on Temperature-Dependent Structural Changes, *Polyhedron*, 2019, **171**, 147–154.
21 I. B. Ustunol, E. K. Coward, E. Quirk and V. H. Grassian, Interaction of Beta-Lactoglobulin and Bovine Serum Albumin with Iron Oxide (α-Fe_2O_3) Nanoparticles in the Presence and Absence of Pre-Adsorbed Phosphate, *Environ. Sci.: Nano*, 2021, **8**, 2811–2823.
22 G. Pietramellara, J. Ascher, F. Borgogni, M. T. Ceccherini, G. Guerri and P. Nannipieri, Extracellular DNA in Soil and Sediment: Fate and Ecological Relevance, *Biol. Fertil. Soils*, 2009, **45**, 219–235.
23 H. Arami, A. Khandhar, D. Liggitt and K. M. Krishnan, In Vivo Delivery, Pharmacokinetics, Biodistribution and Toxicity of Iron Oxide Nanoparticles, *Chem. Soc. Rev.*, 2015, **44**, 8576–8607.
24 I. Holman, M. Whelan, N. Howden, P. Bellamy, N. Willby, M. Rivas-Casado and P. McConvey, Phosphorus in Groundwater—An Overlooked Contributor to Eutrophication?, *Hydrol. Processes*, 2008, **22**, 5121–5127.
25 M. P. Schmidt and C. E. Martínez, Ironing Out Genes in the Environment: An Experimental Study of the DNA–Goethite Interface, *Langmuir*, 2017, **33**, 8525–8532.
26 I. Sit, H. Wu and V. H. Grassian, Environmental Aspects of Oxide Nanoparticles: Probing Oxide Nanoparticle Surface Processes Under Different Environmental Conditions, *Annu. Rev. Anal. Chem.*, 2021, **14**, 489–514.
27 R. A. Fry, K. D. Kwon, S. Komarneni, J. D. Kubicki and K. T. Mueller, Solid-State NMR and Computational Chemistry Study of Mononucleotides Adsorbed to Alumina, *Langmuir*, 2006, **22**, 9281–9286.
28 C. Feuillie, D. A. Sverjensky and R. M. Hazen, Attachment of Ribonucleotides on α-Alumina as a Function of pH, Ionic Strength, and Surface Loading, *Langmuir*, 2015, **31**, 240–248.
29 H. J. Cleaves, C. M. Jonsson, C. L. Jonsson, D. A. Sverjensky and R. M. Hazen, Adsorption of Nucleic Acid Components on Rutile (TiO_2) Surfaces, *Astrobiology*, 2010, **10**, 311–323.
30 I. Sit, E. Quirk, E. Hettiarachchi and V. H. Grassian, Differential Surface Interactions and Surface Templating of Nucleotides (DGMP, DCMP, DAMP, and DTMP) on Oxide Particle Surfaces, *Langmuir*, 2022, **38**, 15038–15049.
31 M. Kosmulski, The pH-Dependent Surface Charging and Points of Zero Charge: V Update, *J. Colloid Interface Sci.*, 2011, **353**, 1–15.
32 I. A. Mudunkotuwa, A. Al Minshid and V. H. Grassian, ATR-FTIR Spectroscopy as a Tool to Probe Surface Adsorption on Nanoparticles at the Liquid-Solid Interface in Environmentally and Biologically Relevant Media, *Analyst*, 2014, **139**, 870–881.
33 S. Bairoliya, J. K. Z. Xing and B. Cao, Extracellular DNA in Environmental Samples: Occurrence, Extraction, Quantification, and Impact on Microbial Biodiversity Assessment, *Appl. Environ. Microbiol.*, 2022, **88**, e01845.
34 A. D. Becke, Density-functional Thermochemistry. III. The Role of Exact Exchange, *J. Chem. Phys.*, 1993, **98**, 5648–5652.
35 C. Lee, W. Yang and R. G. Parr, Development of the Colle-Salvetti Correlation-Energy Formula into a Functional of the Electron Density, *Phys. Rev. B: Condens. Matter Mater. Phys.*, 1988, **37**, 785–789.
36 M. J. Frisch, G. W. Trucks, H. B. Schlegel, G. E. Scuseria, M. A. Robb, J. R. Cheeseman, G. Scalmani, V. Barone, G. A. Petersson, H. Nakatsuji, X. Li, M. Caricato, A. V. Marenich, J. Bloino, B. G. Janesko, R. Gomperts, B. Mennucci, H. P. Hratchian, J. V. Ortiz, A. F. Izmaylov, J. L. Sonnenberg, F. Ding, F. Lipparini, F. Egidi, J. Goings, B. Peng, A. Petrone, T. Henderson, D. Ranasinghe, V. G. Zakrzewski, J. Gao, N. Rega, G. Zheng, W. Liang, M. Hada, M. Ehara, K. Toyota, R. Fukuda, J. Hasegawa, M. Ishida, T. Nakajima, Y. Honda, O. Kitao, H. Nakai, T. Vreven, K. Throssell, J. A. Montgomery Jr., J. E. Peralta, F. Ogliaro, M. J. Bearpark, J. J. Heyd, E. N. Brothers, K. N. Kudin, V. N. Staroverov, T. A. Keith, R. Kobayashi, J. Normand, K. Raghavachari, A. P. Rendell, J. C. Burant, S. S. Iyengar, J. Tomasi, M. Cossi, J. M. Millam, M. Klene, C. Adamo, R. Cammi, J. W. Ochterski, R. L. Martin, K. Morokuma, O. Farkas, J. B. Foresman and D. J. Fox, *Gaussian 16, Revision C.01*, Gaussian, Inc., Wallingford CT, 2016.
37 R. D. J. III, *NIST Computational Chemistry Comparison and Benchmark Database*. NIST Standard Reference Database Numebr 191. **http://cccbdb.nist.gov/**.

38 A. A. Ahmed, S. Gypser, P. Leinweber, D. Freesec and O. Kühn, Infrared Spectroscopic Characterization of Phosphate Binding at the Goethite–Water Interface, *Phys. Chem. Chem. Phys.*, 2019, **21**, 4421–4434.

39 K. Paul, J. D. Kubicki and D. L. Sparks, Sulphate adsorption at the Fe (hydr)oxide-H_2O interface: Comparison of cluster and periodic slab DFT predictions, *Eur. J. Soil Sci.*, 2007, **58**, 978–988.

40 Z. A. Shabarova and A. A. Bogdanov, in Properties of Nucleotides, *Advanced Organic Chemistry of Nucleic Acids*, VCH, Weinheim, Germany, 1994, pp. 93–180.

41 L. El-Mahdaoui, J. F. Neault and H. A. Tajmir-Riahi, Carbohydrate-Nucleotide Interaction. The Effects of Mono- and Disaccharides on the Solution Structure of AMP, DAMP, ATP, GMP, DGMP, and GTP Studied by FTIR Difference Spectroscopy, *J. Inorg. Biochem.*, 1997, **65**, 123–131.

42 J. C. Gonzàlez-Olvera, J. Martìnez-Reyes, E. Gonzàlez-Jasso and R. C. Pless, Determination of p*K*a Values for Deprotonatable Nucleobases in Short Model Oligonucleotides, *Biophys. Chem.*, 2015, **206**, 58–65.

43 W. Yan and C. Jing, Molecular Insights into Glyphosate Adsorption to Goethite Gained from ATR-FTIR, Two-Dimensional Correlation Spectroscopy, and DFT Study, *Environ. Sci. Technol.*, 2018, **52**, 1946–1953.

44 R. R. Wu, C. C. He, L. A. Hamlow, Y.-W. Nei, G. Berden, J. Oomens and M. T. Rodgers, N3 Protonation Induces Base Rotation of 2′-Deoxyadenosine-5′-Monophosphate and Adenosine-5′-Monophosphate, *J. Phys. Chem. B*, 2016, **120**, 4616–4624.

45 H.-A. Tajmir-Riahi and S. Messaoudi, The Effects of Monovalent Cations Li^+, Na^+, K^+, NH^+_4, Rb^+ and Cs^+ on the Solid and Solution Structures of the Nucleic Acid Components. Metal Ion Binding and Sugar Conformation, *J. Biomol. Struct. Dyn.*, 1992, **10**, 345–365.

46 M. Banyay, M. Sarkar and A. Gräslund, A Library of IR Bands of Nucleic Acids in Solution, *Biophys. Chem.*, 2003, **104**, 477–488.

47 V. Barròn and J. Torrenti, Surface Hydroxyl Configuration of Various Crystal Faces of Hematite and Goethite, *J. Colloid Interface Sci.*, 1996, **177**, 407–410.

48 L. O. Filippov, L. A. Silva, A. M. Pereira, L. C. Bastos, J. C. G. Correia, K. Silva, A. Picarra and Y. Foucaud, Molecular Models of Hematite, Goethite, Kaolinite and Quartz: Surface Termination, Ionic Interactions, Nano Topography, and Water Coordination, *Colloids Surf., A*, 2022, **650**, 129585.

49 H. Guo and A. S. Barnard, Thermodynamic Modelling of Nanomorphologies of Hematite and Goethite, *J. Mater. Chem.*, 2011, **21**, 11566–11577.

50 L. Mazeina and A. Navrotsky, Enthalpy of Water Adsorption and Surface Enthalpy of Goethite (α-FeOOH) and Hematite (α-Fe_2O_3), *Chem. Mater.*, 2007, **19**, 825–833.

51 J. Liu, R. Zhu, L. Ma, H. Fu, X. Lin, S. C. Parker and M. Molinari, Adsorption of Phosphate and Cadmium on Iron (Oxyhydr)Oxides: A Comparative Study on Ferrihydrite, Goethite, and Hematite, *Geoderma*, 2021, **383**, 114799.

52 P. Mäkie, G. Westin, P. Persson and L. Österlund, Adsorption of Trimethyl Phosphate on Maghemite, Hematite, and Goethite Nanoparticles, *J. Phys. Chem. A*, 2011, **115**, 8948–8959.

53 M. Villalobos and A. Pérez-Gallegos, Goethite Surface Reactivity: A Macroscopic Investigation Unifying Proton, Chromate, Carbonate and Lead (II) Adsorption, *J. Colloid Interface Sci.*, 2008, **326**, 307–323.

54 A. Omoike, J. Chorover, K. Kwon and J. D. Kubicki, Adhesion of Bacterial Exopolymers to α-FeOOH: Inner-Sphere Complexation of Phosphodiester Groups, *Langmuir*, 2004, **20**, 11108–11114.